Current Biology 19, 1599–1607, October 13, 2009 ©2009 Elsevier Ltd All rights reserved DOI 10.1016/j.cub.2009.08.045

Article

The CIL-1 PI 5-Phosphatase Localizes TRP Polycystins to Cilia and Activates Sperm in *C. elegans*

Young-Kyung Bae,[1,4] Eunsoo Kim,[2] Steven W. L'Hernault,[3] and Maureen M. Barr[1,*]

[1]Department of Genetics, Rutgers University, the State University of New Jersey, Piscataway, NJ 08854, USA

[2]Department of Biochemistry and Molecular Biology, Dalhousie University, 5850 College Street, Halifax NS B3H 1X5, Canada

[3]Department of Biology, Emory University, Atlanta GA 30322, USA

Summary

Background: *C. elegans* male sexual behaviors include chemotaxis and response to hermaphrodites, backing, turning, vulva location, spicule insertion, and sperm transfer, culminating in cross-fertilization of hermaphrodite oocytes with male sperm. The LOV-1 and PKD-2 transient receptor potential polycystin (TRPP) complex localizes to ciliated endings of *C. elegans* male-specific sensory neurons and mediates several aspects of male mating behavior. TRPP complex ciliary localization and sensory function are evolutionarily conserved. A genetic screen for *C. elegans* mutants with PKD-2 ciliary localization (Cil) defects led to the isolation of a mutation in the *cil-1* gene.

Results: Here, we report that a phosphoinositide (PI) 5-phosphatase, CIL-1, regulates TRPP complex ciliary receptor localization and sperm activation. *cil-1* does not regulate the localization of other ciliary proteins, including intraflagellar transport (IFT) components, sensory receptors, or other TRP channels in different cell types. Rather, *cil-1* specifically controls TRPP complex trafficking in male-specific sensory neurons and does so in a cell-autonomous fashion. In these cells, *cil-1* is required for normal PI(3)P distribution, indicating that a balance between PI(3,5)P2 and PI(3)P is important for TRPP localization. *cil-1* mutants are infertile because of sperm activation and motility defects. In sperm, the CIL-1 5-phosphatase and a wortmannin-sensitive PI 3-kinase act antagonistically to regulate the conversion of sessile spermatids into motile spermatozoa, implicating PI(3,4,5)P3 signaling in nematode sperm activation.

Conclusion: Our studies identify the CIL-1 5-phosphatase as a key regulator of PI metabolism in cell types that are important in several aspects of male reproductive biology.

Introduction

Phosphoinositides (PIs) and their phosphatases and kinases play pivotal roles in receptor trafficking as well as in membrane organelle biogenesis and transport, endocytosis, cytoskeleton dynamics, signal transduction, cell motility, and channel activity modulation [1, 2]. Many sensory receptors localize to ciliary membrane, which serve as cellular antennae and function in development, signaling, and physiology. Whether PIs and PI-generating enzymes regulate ciliary receptor trafficking is unknown.

The nematode *Caenorhabditis elegans* is a powerful model for the study of molecular mechanisms required for ciliary receptor trafficking. The *C. elegans* transient receptor potential polycystin (TRPP) complex proteins LOV-1 (TRPP1) and PKD-2 (TRPP2) localize to sensory cilia [3, 4]. Autosomal-dominant polycystic kidney disease (ADPKD) is caused by mutations in the TRPP1 and TRPP2 genes [5]. Since the discovery of LOV-1 and PKD-2 in cilia of *C. elegans* male-specific sensory neurons, TRPPs have been found in primary cilia or flagella in organisms ranging from alga to man, hinting at an evolutionarily conserved mechanism regulating TRPP ciliary localization (reviewed in [6]).

In diverse species, TRPP family proteins serve reproductive functions [7–12]. *C. elegans* LOV-1 and PKD-2 function in male mating behaviors. *pkd-2* appears to be expressed solely in the male nervous system and not sperm, as judged by antibody staining [4]. In contrast to mammalian and *Drosophila* sperm, nematode sperm are not flagellated and do not possess an actin or tubulin cytoskeleton (reviewed in [13]). Instead, each sperm extends a single pseudopod enriched with major sperm protein (MSP). MSP is used to assemble a filamentous network required for amoeboid motility and fertilization. Screens have identified genes required for spermatogenesis, hermaphrodite or male sperm activation, and sperm function. Signaling pathways involved in sperm activation in both males and hermaphrodites are not known.

PKD-2 ciliary localization requires vesicular trafficking and utilizes both general and cell-type-specific factors [14]. General factors include the clathrin-coated vesicle adaptor protein-1 (AP-1) UNC-101 and the intraflagellar transport (IFT) machinery. Cell-type-specific PKD-2 localization factors include LOV-1 and the STAM-Hrs (signal-transducing adaptor molecule and hepatocyte growth factor-regulated tyrosine kinase substrate) complex [14, 15]. We performed a genetic screen for *C. elegans* mutants with PKD-2 ciliary localization (Cil) defects [16]. Here, we identify CIL-1, a PI 5-phosphatase that regulates TRPP complex localization. *cil-1* is also a positive regulator of sperm activation and motility. Using genetically encoded PI-indicators and pharmacological approaches, we determine that CIL-1 hydrolyses PI(3,5)P2 and PI(3,4,5)P3 in male-specific sensory neurons and sperm, respectively. We conclude that CIL-1 acts in multiple tissues that are important for male reproductive biology, thereby controlling diverse cellular processes as an in vivo PI-metabolizing enzyme.

Results

cil-1 Is Required for LOV-1 and PKD-2 Localization

In wild-type (WT), PKD-2::GFP localizes to cell bodies and ciliary endings of 21 male-specific neurons in the head (cephalic CEMs) and tail (ray RnBs and hook HOB) ([14], Figures 1A–1D). In *my15* mutants, PKD-2::GFP is distributed throughout these male-specific neurons including dendrites, axons, cell bodies, and cilia (Figures 1E and 1F). *cil-1* is not required for neuronal cell fate or development of *pkd-2*-expressing

*Correspondence: barr@biology.rutgers.edu

[4]Present address: California Institute of Technology, Division of Biology MC 114-96, Pasadena, CA 91125, USA

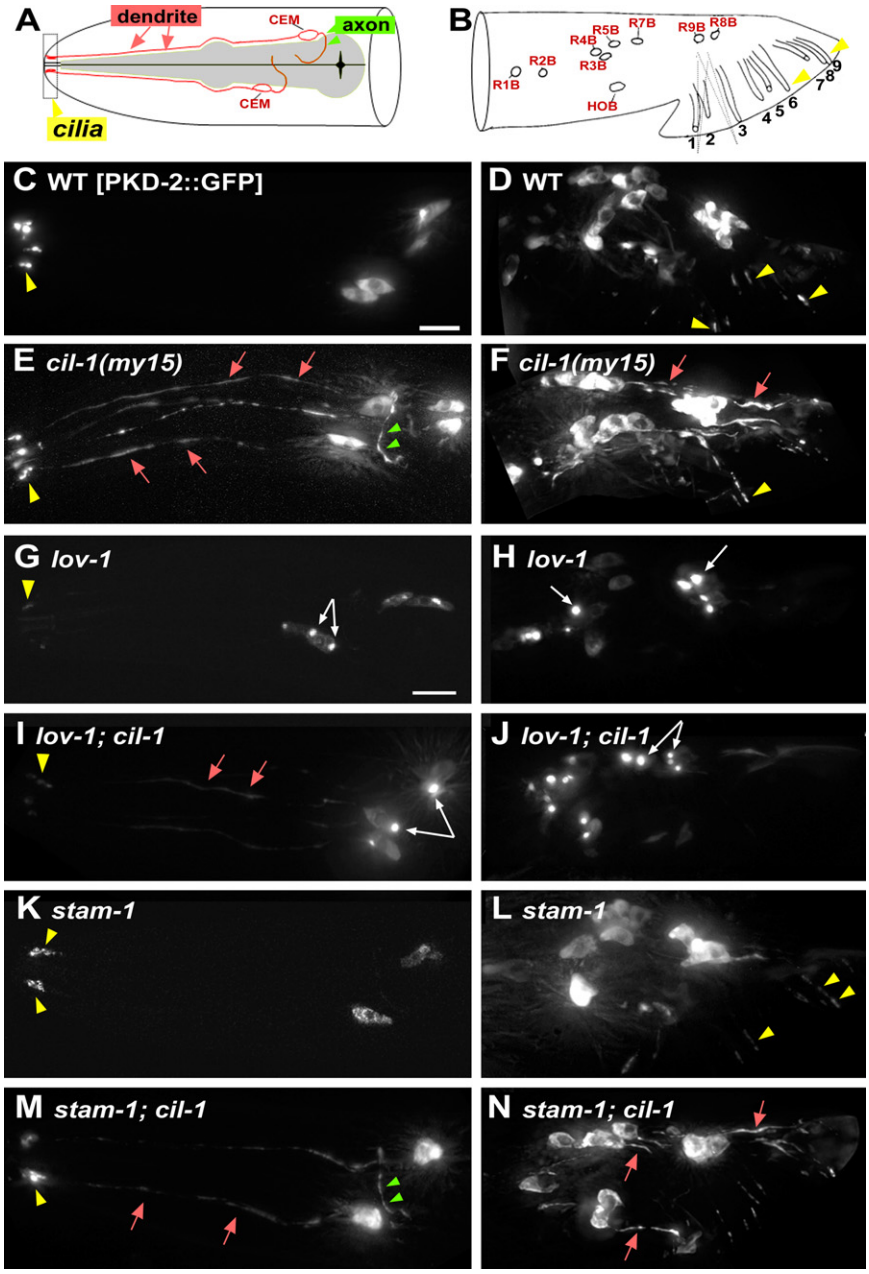

Figure 1. *cil-1* Is Required for TRP Polycystin Complex Localization

cil-1 acts between *lov-1* and *stam-1* in ray B neurons. White arrows show cell bodies, yellow arrowheads show cilia, red arrows show dendrites, and green arrowheads show axons. Scale bars represent 10 μm.

(A and B) Cartoons illustrating locations and structure of *pkd-2*-expressing neurons in *C. elegans* male head (A) and tail (B). The head CEMs and tail ray neurons are bilateral, and only one side of the animal is shown. Modified with permission from [37].

(C and D) In a WT male, PKD-2::GFP localizes to cilia and neuronal cell bodies of CEM, ray B (RnB), and hook B (HOB) neurons.

(E and F) In *cil-1(my15)* males, PKD-2::GFP is abnormally distributed along neurons including dendrites and axons. PKD-2::GFP in ciliary regions appears to be WT.

(G) In *lov-1* CEMs, PKD-2::GFP accumulates in cell bodies and weakly labels in cilia.

(H) In *lov-1* RnBs, PKD-2::GFP accumulates in cell bodies and is not detectable in cilia.

(I) In *cil-1; lov-1* CEMs, PKD-2::GFP aggregates in cell bodies and distributes along dendrites and cilia.

(J) In *cil-1; lov-1* RnBs, PKD-2::GFP forms bright aggregates in the cell bodies, similar to the *lov-1* single mutant.

(K) In *stam-1* CEMs, PKD-2::GFP accumulates in ciliary regions.

(L) In *stam-1* RnBs, PKD-2::GFP accumulates in the ciliary regions and distal dendrites [15].

(M) In *stam-1; cil-1* CEMs, PKD-2::GFP localizes to dendrites and axons and sometimes accumulates ciliary bases.

(N) In *stam-1; cil-1* RnBs, PKD-2::GFP is distributed to dendritic and axonal processes, similar to *cil-1* single mutants.

neurons as judged by reporters including transcriptional and soluble P*pkd-2::*GFP, OSM-6::GFP (data not shown), P*pkd-2:*SNB-1:GFP (see Figure S1, available online), and fluorescent-protein-tagged PI-markers (Figure S4). P*pkd-2*::GFP and endogenous *pkd-2* mRNA levels are unaltered in *my15* animals as judged by qRT-PCR (data not shown), indicating that *my15* may affect PKD-2 protein expression or stability but not gene expression. In WT and *my15* dendrites, small PKD-2::GFP particles move bidirectionally (Movies S1 and S2), indicating that a pool of PKD-2::GFP is properly trafficked in *my15* dendrites. Moreover, PKD-2::GFP distribution in the *my15* ciliary region appears normal, despite abnormally increased dendritic and axonal distributions (Figures 1E and 1F, [16]).

We examined the distribution of additional GFP-tagged ciliary proteins, including functional LOV-1::GFP ([15], Figures S1A–S1D); a TRP-vanilloid, OSM-9; a G protein-coupled receptor (GPCR), ODR-10; an IFT B-complex polypeptide, OSM-6; and an IFT modulator, BBS-5. Only LOV-1::GFP is abnormally distributed to dendritic and axonal processes in *my15* sensory neurons (Figures S1C and S1D). We also examined the localization of the presynaptic marker synaptobrevin P*pkd-2*::SNB-1::GFP [17]. In WT and *my15* males, SNB-1::GFP labels presynaptic puncta along axonal processes (Figures S1E and S1F), indicating that *cil-1* does not grossly affect axonal targeting. *my15* mutants are normal in lipophilic DiI dye filling of ciliated sensory neurons, chemotaxis to diacetyl, dauer formation, and osmotic avoidance (data not shown). We conclude that *cil-1* is specifically required for localization of the TRPP complex but not for general receptor trafficking, ciliogenesis, neuronal polarization, or sensation.

lov-1, *pkd-2*, and a subset of Cil mutants are response and location of vulva (Lov) defective during male mating [3, 4, 16]. *my15* males exhibit normal response and vulva location behaviors (Figure S1, [16]), which may be explained by the presence of PKD-2::GFP in cilia. *cil-1* double- or triple-homozygous or transheterozygous mutants with *pkd-2* and *lov-1* did not alter male mating efficiency, indicating that *cil-1* is not a genetic modifier of the *C. elegans* TRPP genes (data

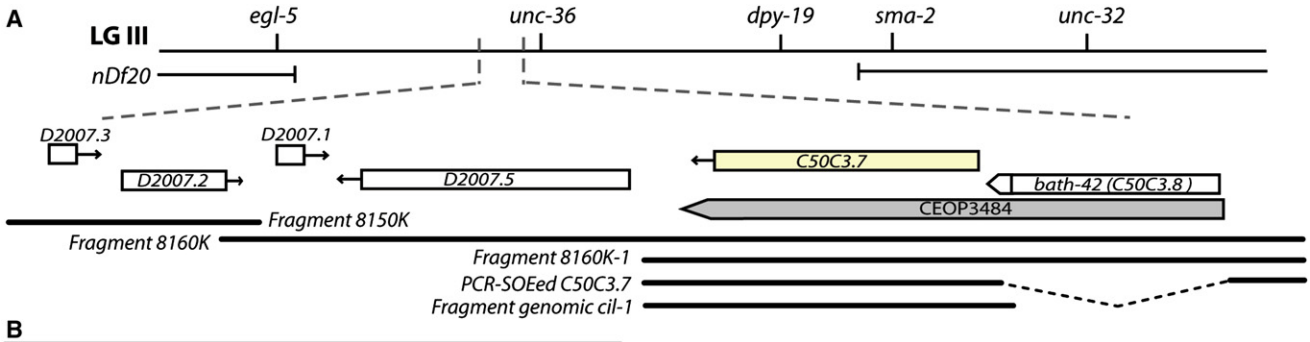

B

injected fragments	rescue? (rescuing/total lines)	
	Cil	Spe (brood size)
8150K + 8160K	+ (2/2)	ND
8160K	+ (4/5)	ND
8160K-1	+ (6/6)	ND
PCR-SOEed C50C3.7	+ (2/2)	+ (2/2)
genomic cil-1	+ (1/1)	- (0/1)
Ppkd-2::cil-1(cDNA)::tdtomato	+ (3/5)	- (0/5)

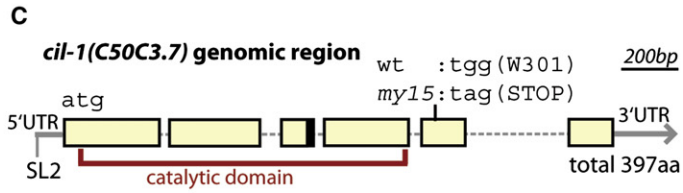

Figure 2. *cil-1/C50C3.7* Encodes a Phosphoinositide 5-Phosphatase

(A) Genetic and physical maps of the region of LG III encompassing the *cil-1* locus. Positions of rescuing genomic fragments are aligned approximately to the physical map.

(B) Summary table for rescue effects of injected *cil-1(my15)* lines. The Spe phenotype was scored by hermaphroditic brood size.

(C) C50C3.7 is the gene mutated in *cil-1(my15)*. Six blank boxes indicate exons connected with five introns. *my15* is a nonsense mutation in the fifth exon (301st amino acid). The black box at the end of the third exon indicates the position of alternative splicing for the short form C50C3.7b. C50C3.7a encodes a phosphoinositide 5-phosphatase, and the catalytic domain is indicated in red.

not shown). Although mating behaviors appear normal, *my15* males are largely infertile and produce few offspring because of a sperm (Spe) defect, which will be discussed later.

cil-1 Acts between *lov-1* and *stam-1* in RnB Ray Neurons

We previously showed that TRPP complex formation is important for trafficking [14]. In a *lov-1* mutant, PKD-2::GFP forms aggregates in cell bodies and localizes to cilia at a reduced level (Figures 1G and 1H). In *lov-1; cil-1* CEM neurons (Figure 1I), the PKD-2::GFP localization phenotype is additive: bright aggregates in the cell bodies (*lov-1* phenotype; white arrows) and mislocalization to the dendrites and axons (*cil-1* phenotype), albeit at reduced levels (red arrows). In *lov-1; cil-1* RnB neurons (Figure 1J), the PKD-2::GFP localization phenotype resembles that of *lov-1* but not *cil-1*: aggregates in the cell body and absence from dendritic and ciliary compartments. This strict requirement of *lov-1* in RnB as compared to CEM neurons has been previously shown for PKD-2 ciliary targeting [14]. The basis of this cell-type specificity is unknown, but may be due to differences in protein trafficking mechanisms or structural differences between CEM and RnB neurons.

PKD-2 ciliary abundance is tightly controlled. STAM and Hrs mediate PKD-2 and LOV-1 downregulation via transport from early endosomes to endosomal sorting complexes (ESCRT) [15]. Reducing *stam-1* or *hgrs-1* function results in PKD-2::GFP and LOV-1::GFP accumulation at the ciliary base (Figure 1K and 1L, [15]). In CEM neurons of a *stam-1(ok406); cil-1(my15)* double mutant (Figure 1M), the PKD-2::GFP localization phenotype is additive. In *stam-1; cil-1* RnB neurons (Figure 1N), PKD-2::GFP is distributed evenly throughout, similar to *cil-1* single mutants. We conclude that, in RnB neurons, *cil-1* acts after *lov-1* but before *stam-1*. In CEMs, the *lov-1; cil-1* and *cil-1; stam-1* phenotype is complex, making it difficult to place *lov-1*, *cil-1*, and *stam-1* in a linear or parallel pathway.

cil-1 Encodes a Phosphoinositide 5-Phosphatase that Acts Cell Autonomously

The smallest rescuing genomic fragment for both the Cil and Spe phenotypes (8160K-1, Figures 2A and 2B) contains two genes, C50C3.7 and *bath-42* in the operon CEOP3484. The *bath-42(tm2360)* deletion mutant is nonCil and nonSpe (data not shown). A construct containing 2.2 kb 5′UTR of the *bath-42* and the C50C3.7 genomic region including the 3′UTR rescues both Cil and Spe phenotypes of *my15* (PCR-SOEed C50C3.7, Figures 2A and 2B). Sequencing analysis of *my15* genomic DNA identified a G→A transition that converts Trp^{301} (TGG) to a stop codon (TAG) in the 5th exon of C50C3.7 (Figure 2A). From both WT and *my15* cDNA pools, reverse transcriptase PCR (RT-PCR) identified two *cil-1* cDNAs (long C50C3.7a and short C50C3.7b). The short form (C50C3.7b) is generated by alternative splicing within the third intron, introducing a stop codon at the 124th amino acid before the *my15*-induced lesion. P*pkd-2*::CIL-1a(C50C3.7a)::td Tomato fully rescues the *cil-1(my15)* Cil but not the Spe phenotype (Figures 2A and 2B), which is not surprising given that *pkd-2* is not expressed in sperm. In contrast, expression of C50C3.7a with an intestinal promoter fails to rescue the Cil phenotype (data not shown). We did not attempt to rescue the *cil-1(my15)* Spe phenotype by using cell-type-specific promoters because transgenes are often silenced in the

germline. We conclude that C50C3.7 is the gene mutated in *cil-1(my15)* animals and that CIL-1 acts autonomously in male-specific neurons to control TRPP localization.

cil-1 encodes a phosphoinositide (PI) 5-phosphatase (referred to as 5-phosphatase), which removes the D-5 phosphate from the inositol ring of membrane-associated PI or soluble inositol phosphates. The 5-phosphatase family comprises ten mammalian, four yeast, and five *C. elegans* enzymes. Phylogenetic analysis of the 5-phosphatase catalytic domain and/or of the presence or absence of adjacent domains reveals that CIL-1 is closely associated with two mammalian 5-phosphatases: SKIP (*s*keletal muscle and *k*idney-enriched *i*nositol *p*hosphatase) and PIPP (*p*roline-rich *i*nositol *p*olyphosphate *p*hosphatase). CIL-1, SKIP, and PIPP belong to the SKICH (SKIP carboxyl homology) subfamily, which contains a C-terminal SKICH-like domain (Figures S2A and S2D) and mediates protein localization [18].

The *C. elegans* genome encodes five 5-phosphatase genes: *ipp-5*, *unc-26*, *ocrl-1*, *cil-1*/C50C3.7, and T25B9.10. *ipp-5* (type I) negatively regulates ovulation by inhibiting inositol 1,4,5-triphosphate (IP3) signaling in the spermatheca [19]. IP3 signaling also regulates mating behavior steps of turning, spicule insertion, and sperm transfer [20]. *unc-26* (synaptojanin) is required for synaptic vesicle endocytosis and recycling, with mutants exhibiting uncoordinated movements [21]. Neither the *ipp-5* nor the *unc-26* mutant is Cil or Spe defective, and *cil-1(my15)* mutants are normal in ovulation, locomotion, male turning, spicule insertion, and sperm transfer, ruling out possible overlapping functions (data not shown).

CIL-1 contains two conserved 5-phosphatase motifs in its catalytic domain (Figure S2B). We introduced a missense mutation in a known critical residue of 5-phosphatase motif (CIL-1^{N175A}, Figure S2B, red arrowhead). P*pkd-2*::CIL-1^{N175A}::tdTomato failed to rescue the *my15* Cil phenotype, indicating that phosphatase catalytic activity is required for CIL-1 function.

In male neurons, the rescuing P*pkd-2*::CIL-1::tdTomato is distributed in cilia, dendrites, axons, cell bodies with occasional small puncta, and weakly in nuclei (Figure S3D), and it is often visible as bright dots at ciliary bases of ray neurons (Figure S3E), suggesting CIL-1 function in ciliary regions. In the intestine, P*vha-6*::CIL-1::GFP localizes to cytoplasmic reticular structures (Figure S3F).

CIL-1 Regulates PI(3,4)P2/PI(3,4,5)P3 and PI(3)P but Not PI(4,5)P2 Levels

Seven PI species are generated by the reversible phosphorylation and dephosphorylation. To determine what PI species are CIL-1 substrates, we expressed genetically encoded biosensors to detect changes in specific PI lipid concentrations in male-specific sensory neurons and the intestine. We observed obvious differences in PI(3)P Hrs(2xFYVE) and PI(3,4)P2/PI(3,4,5)P3 AKT(PH), but not PI(4,5)P2 (PH domain of PLC-delta) markers between WT and *cil-1(my15)* animals. In the WT intestine, PI(3)P is primarily found in tubulovesicular structures without any plasma membrane (PM) enrichment, similar to the CIL-1 distribution pattern (compare Figure 3A with Figure S3F). In the *cil-1* intestine, PI(3)P is severely disrupted, with a diffuse pattern in the cytoplasm (Figure 3D). In WT intestine, PI(3,4)P2/PI(3,4,5)P3 is found in tubulovesicular structures and enriched at the PM (Figure 3B, arrowheads and arrow). In *cil-1(my15)* mutants, the PI(3,4)P2/PI(3,4,5)P3 marker labels no distinct structure, appearing diffuse in the cytoplasm with no PM enrichment. A similar pattern has been reported in *C. elegans let-512/vps-34* PI 3-kinase mutants, in which PI(3)P generation is reduced [22]. In both WT and *cil-1(my15)* intestine, PI(4,5)P2 is enriched at the apical PM lining the intestinal lumen as well as basolateral PM (Figures 3C–3F). These data indicate that CIL-1 displays in vivo phosphatase activity toward PI(3,4,5)P3 and PI(3,5)P2 in the intestine.

In male-specific sensory neurons, we observe differences in PI(3)P distribution (Figures 3G and 3H), but not PI(3,4)P2/PI(3,4,5)P3 or PI(4,5)P2 markers in *cil-1(my15)* males (Figure S4). In WT neurons, the PI(3)P marker is enriched in nuclei and small puncta in the cell bodies, but rarely in dendritic and ciliary regions (Figures 3G and 3G′), with only 1/13 animals displaying detectable expression in dendrites and cilia. In *cil-1(my15),* the PI(3)P marker decorates dendritic processes and cilia (16/27 animals) in addition to the enrichment in the nuclei and cell bodies (Figures 3H and 4H′). The PI(3)P marker is distinctly bright at *cil-1(my15)* ciliary bases (Figure 3H, inset), hinting that loss of CIL-1 perturbs PI(3)P distribution in this region. These data suggest that CIL-1 displays a tissue-specific substrate preference toward PI(3,5)P2 in male sensory neurons.

Because PI(3)P localizes to early endosomes, we examined the distribution of early endosomal proteins. RAB-5 is an early endosomal protein that recruits and activates PI(3)P-generating PI 3-kinases [23]. STAM-1 colocalizes with RAB-5 in *C. elegans* male-specific sensory neurons and promotes polycystin trafficking from early endosomes to the ESCRT complex [15]. In WT and *cil-1(my15)* animals, RAB-5 and STAM-1 localize to small puncta in the cell bodies, axons, and dendrites (Figures S4G–S4J), indicating that *cil-1* does not modify the overall organization of early endosomes.

cil-1 Mutants Are Sperm Defective

cil-1(my15) hermaphrodites exhibit a drastic reduction in brood size (4.85% of WT) (Figures S5A), which is due to a spermatogenesis defect (Spe) based on the following observations: (1) a *my15* hermaphrodite lays 200–300 unfertilized eggs, which is comparable to the number of WT fertilized eggs (Figures S5A); (2) *my15* male germline architecture and early stages of spermatogenesis (data not shown), hermaphrodite oocyte maturation, and ovulation appear normal (Figures S4D and S4E); (3) *my15* hermaphrodites contain endomitotic cells without eggshells in the uterus (Figures S5F and S5G); (4) the *my15* fertility defect is completely rescued when *my15* hermaphrodites are mated with WT males (Figures S5B); and (5) *my15* males fail to sire cross progeny without overt behavioral defects in mating behaviors (Figures S5C and S1G). We conclude that *cil-1* is required for sperm function in both hermaphrodites and males.

A Spe phenotype may arise from developmental defects in spermatogenesis, sperm activation (spermiogenesis), sperm motility, or sperm-egg interactions. *my15* male gonads have normal DAPI staining patterns for each meiotic stage in the gonad and normal number of spermatids (inactive 1N sperm) (data not shown). Thus, *cil-1* is not required for early spermatogenesis up to spermatid production. Defective sperm-egg interactions are the basis of Spe phenotypes in *spe-9*, *spe-38*, *trp-3/spe-41*, and *spe-42* (Figure 4A) (reviewed in [13]). In these Spe mutants, male-derived sperm normally develop, activate, crawl, and compete with endogenous hermaphroditic sperm but cannot fertilize an oocyte. However, *my15* male-derived sperm do not compete with endogenous hermaphrodite-derived sperm, as reflected by a large number

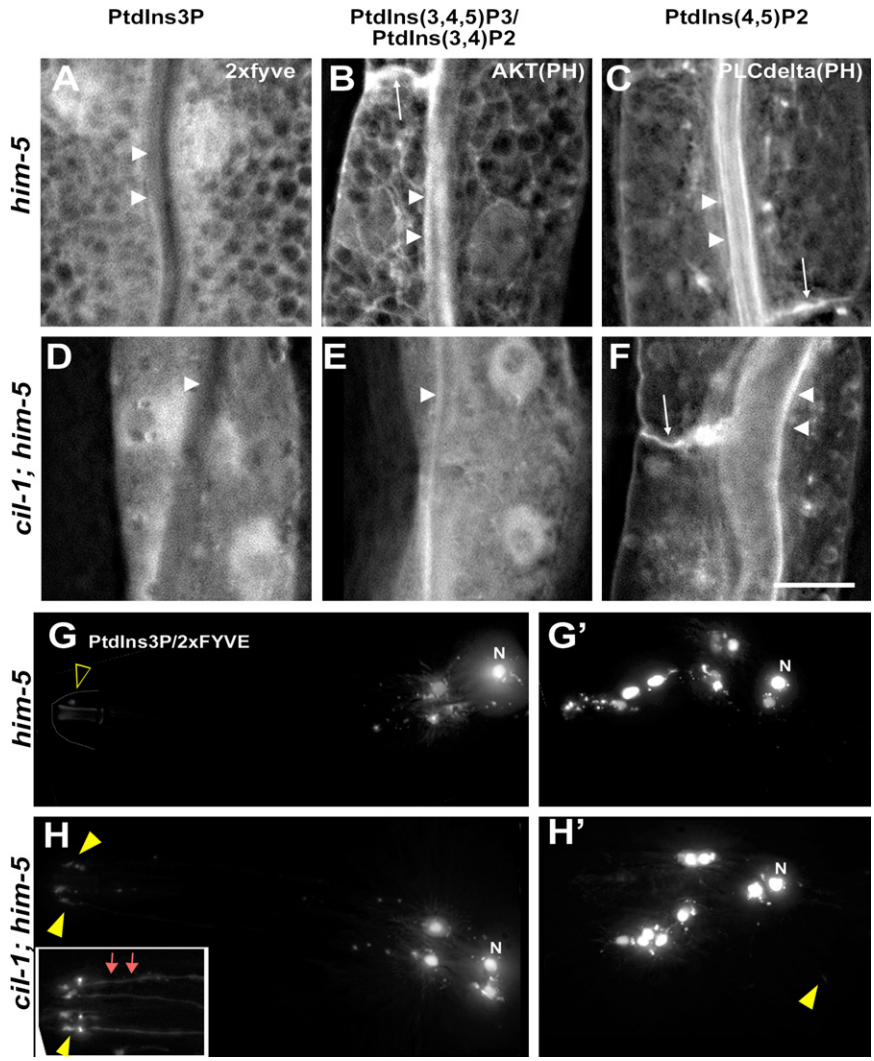

Figure 3. *cil-1* Regulates PI(3,5)P2 and PI(3,4,5)P3 Subcellular Distribution

GFP-tagged PI-specific markers in the intestine of adult males are 2xFYVE for PI(3)P, AKT(PH domain) for PI(3,4,5)P3 and PI(3,4)P2, and PLC-delta (PH domain) for PI(4,5)P2.

(A–C) In the WT intestine: (A) PI(3)P labels mesh-like, tubulovesicular structures in the cytoplasm without obvious PM labeling. (B) PI(3,4,5)P3 and PI(3,4)P2 label similar tubulovesicular structures as well as the apical (arrowheads) and basolateral (arrow) PM. (C) PI(4,5)P2 predominantly labels the apical (arrowheads) in addition to the basolateral (arrow) PM.

(D–F) In the *cil-1(my15)* intestine: (D) PI(3)P appears soluble in the cytoplasm. (E) PI(3,4,5)P3 and PI(3,4)P2 lose their tubulovesicular pattern, appearing diffuse in the cytoplasm. The PM labeling is less prominent in *cil-1* mutants (arrowheads). (F) PI(4,5)P2 remains enriched in the PM. The scale bar represents 10 μm.

(G and H) tdTomato-tagged 2xFYVE domain [PI(3)P marker] expression in male-specific neurons of WT and *cil-1(my15)*. (G) In WT CEMs, the PI(3)P marker is bright in the nuclei (denoted as "N"), labels small puncta in the cell bodies, but is almost absent from cilia (blank yellow arrowhead). (G′) Similarly, in WT RnBs, the PI(3)P marker is confined to cell bodies (nuclei and small puncta). (H) In *cil-1(my15)* CEMs, the PI(3)P marker is visible in cilia and dendrites (arrows) in addition to cell bodies. The inset shows PI(3)P marker labeling ciliary and dendritic regions. (H′) In *cil-1(my15)* RnBs, the PI(3)P marker is occasionally visible in cilia (yellow arrowhead) in addition to cell bodies.

of self-progeny and extremely low mating efficiency (ME) (1.9%, Figure S5C). ME of WT males is higher with *my15* hermaphrodites (~95%) than control hermaphrodites (58%) (Figure S5C), illustrating that *my15* endogenous sperm are nearly incapable of competing with WT male-derived sperm. Hence, *cil-1* acts in events between spermatid production and sperm-egg interactions.

cil-1 Is Required for Sperm Activation and Motility

During sperm activation, a round spermatid develops into a motile spermatozoon with a pseudopod (Figure 4A). This process can be mimicked in vitro by chemical activators such as the ionophore monensin or Pronase (reviewed in [13]). Within 15 min of Pronase application, the majority of WT male spermatids (63.4%, n = 347) extend pseudopods (Figures 4B and 4B′), and the average length of spermatozoa is 8.13 ± 1.11 μm (± standard deviation [SD], n = 95) (Figure 4B′). In contrast, only 47.8% (n = 128) of *my15* male spermatids develop pseudopods after Pronase activation (Figures 4C and 4C′), with a significantly shorter spermatozoa length (6.37 ± 0.61μm [n = 112], p = 1.09E-28, Figure 4C′). The diameter of *my15* spermatids is also slightly smaller (6.22 ± 0.54 μm, n = 136) than WT (6.73 ± 0.65 μm, n = 110, p = 8.08E-07). We also observe in vivo sperm activation defects in *my15* hermaphrodites. In wild-type, 83.3% of spermatozoa possess pseudopods (n = 36, Figure 4B″), whereas only 8.3% do in *my15* mutants (n = 72, Figure 4C″). When present, *my15* pseudopods are significantly shorter (average length of longest axes of sperm; 4.32 ± 0.38 μm, n = 6) than WT (5.43 ± 0.62 μm, n = 37, p = 1.14E-4). Thus, *cil-1* positively regulates sperm activation in vitro and in vivo.

To measure *my15* sperm motility, we performed a time-lapse sperm-tracking assay. WT male sperm crawl from the uterus to the spermatheca over time, with the majority localizing at the spermatheca in 16 hr (Figure 4D). In contrast, *my15* sperm are not observed in the spermatheca at 16 hr despite being present at 4 hr (Figure 4D). These data suggest that *my15* sperm display reduced motility and, consequently, are not retained in the hermaphrodite spermatheca. After in vitro chemical activation with monensin, WT sperm crawl at the rate of 0.33 ± 0.04 μm/s (n = 7) on glass slides (Movie S3), whereas isolated *my15* sperm are immotile (Movie S4).

Sperm activation involves fusion of membranous organelles (MOs) to the PM, exocytosis, and pseudopod extension (reviewed in [13]). To examine MOs, we used the MO-specific monoclonal antibody 1CB4 [24] and the lipophilic dye FM1-43 [25]. In WT, the majority of MOs are found at the cell periphery of round spermatids (Figure 4H). After activation, MOs are excluded from the pseudopod (Figure 4H′). In *my15* sperm, 1CB4 staining for MO morphology and localization before and after activation appears to be WT (Figures 4I and

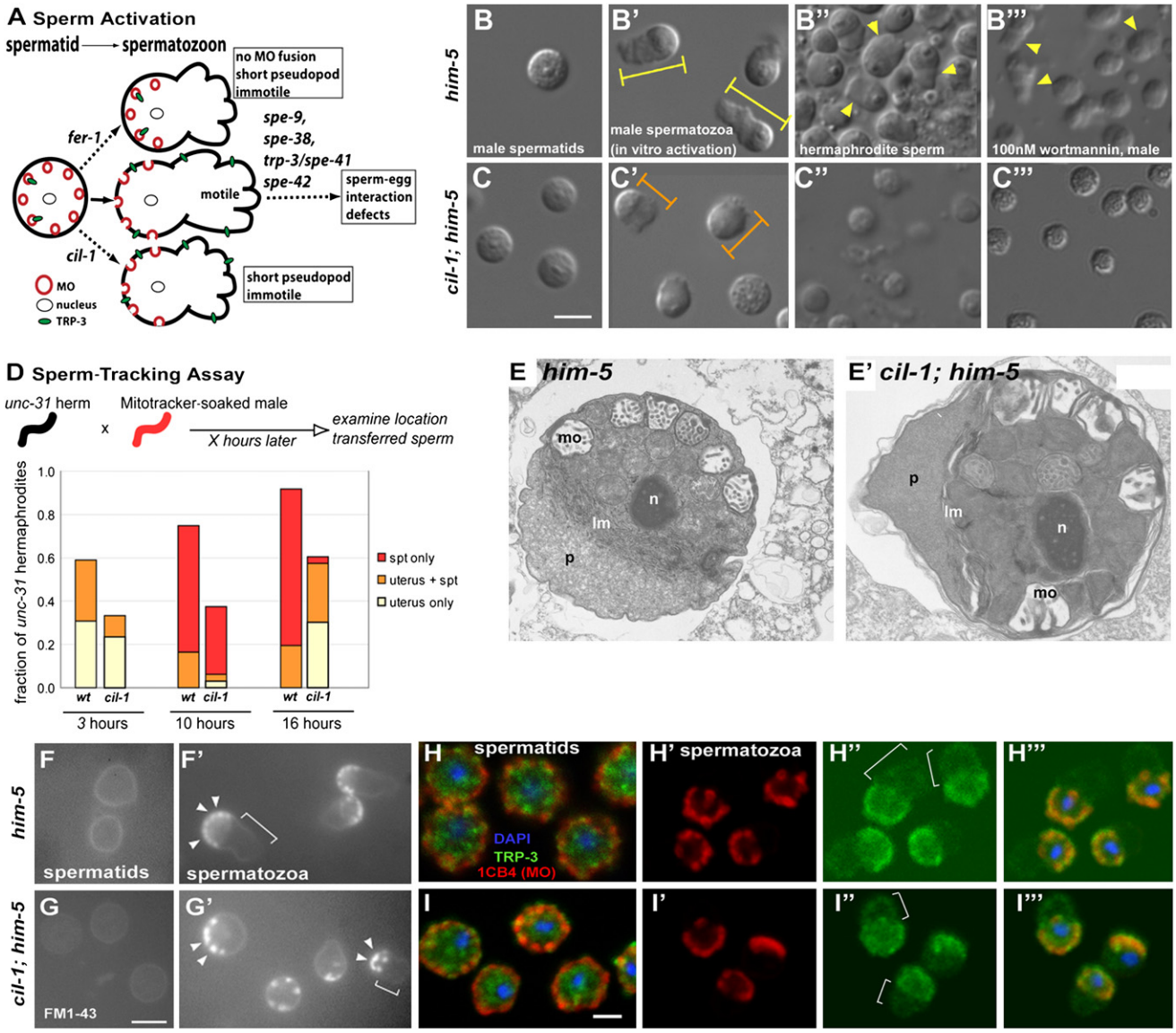

Figure 4. *cil-1* Positively Regulates Sperm Activation and Motility

(A) *C. elegans* sperm activation summarized in this illustration depicting pathways and genes functioning during sperm activation and fertilization. In a spermatid, MOs containing a TRPC receptor, TRP-3, are located just below the PM. During WT activation (solid arrow), MOs fuse to the PM and a pseudopod develops, producing a motile spermatozoon. In *fer-1* mutant sperm (upper dotted arrow), MOs do not fuse with the PM and a short pseudopod forms, resulting in immotile sperm. A *cil-1* mutant sperm (lower dotted arrow) is normal in MO fusion but develops into immotile spermatozoon with a short pseudopod. TRPC TRP-3 translocation from MO to the PM appears normal in *cil-1* mutant sperm. *spe-9*, *spe-38*, *spe-41/trp-3*, and *spe-42* encode various membrane proteins required for sperm-egg interactions. Loss of any of these genes results in motile but infertile spermatozoa.

(B and C) Nomarski images of isolated male-derived sperm before and after in vitro activation and endogenously activated hermaphrodite-derived sperm. (B) shows a round WT spermatid. (B′) shows WT spermatozoa after 15 min of pronase activation. Spermatozoa extend full-length pseudopods (yellow arrowheads). Yellow bars depict the length of WT spermatozoa measured. (B″) shows WT hermaphrodite-derived sperm that are endogenously activated. (B‴) WT male-derived sperm are activated to spermatozoa with pseudopods (arrow arrowheads) within 10 min of 100 nM wortmannin application. (C) *cil-1(my15)* mutant spermatids before activation are slightly smaller than WT spermatids. (C′) Upon activation, *cil-1* mutant sperm develop stubby pseudopods. The length of sperm is indicated with orange bars shorter than WT (compare to yellow bars). (C″) Hermaphrodite-derived sperm from the *cil-1(my15)* mutant occasionally develop short pseudopods. (C‴) *my15* male-derived sperm are not activated by 100nM wortmannin but exhibit subtle morphological changes.

(D) Sperm-tracking assay. The majority of WT male-derived sperm are deposited and retained within the spermatheca in the hermaphroditic reproductive tract at 10 and 16 hr. In contrast, *cil-1(my15)* male-derived sperm are not found in the spermatheca at 16 hr. spt denotes spermatheca.

(E and E′) Ultrastructure of *him-5(e1490)* (E) and *cil-1(my15) him-5(e1490)* (E′) spontaneously activated spermatozoa.

The following abbreviations are used: lm, laminar membranes; mo, membranous organelles; n, nucleus; and p, pseudopod. Although the cytoplasm in this *cil-1* pseudopod (compare E to E′) appears denser than that of the WT control, the significance, if any, of this observation is unclear.

(F and G) Monitoring MO fusion during sperm activation with a lipophilic FM1-43 dye. (F) The PM of WT spermatids is stained with FM1-43. (F′) In WT spermatozoa, the dye concentrates at the MO fusion sites. MO fusion events are restricted to the PM of cell body (arrowheads) but not pseudopod (bracket). (G) FM1-43 dye marks the PM of *cil-1* spermatids. (G′) In short *my15* spermatozoa with visible pseudopods, MO fusion sites are concentrated on the cell body (arrowheads) and excluded from the pseudopod PM (bracket).

(H and I) Immunohistochemistry of sperm with the MO antibody 1CB4 (red), anti-TRP-3 (green), and DAPI (blue). The triple-labeled images were generated by overlaying three confocal images from the same Z section. (H) In WT spermatids, MOs (red) are located around the cell periphery below the PM. The location

4I′). In both WT and *my15*, FM1-43 labels the PM of the round spermatids (Figures 4F and 4G) and, after activation, concentrates at the site of membrane fusion on the spermatozoon cell body (Figures 4F′ and 4G′, arrowheads). *cil-1* is not essential for MO morphology, localization, or fusion.

The ultrastructure of *my15* sperm is largely unaffected as determined by transmission electron microscopy (TEM). The early stages of spermatogenesis in WT and *my15* appear very similar (data not shown). Occasionally, dissected males will produce spontaneously activated spermatozoa, and we examined such cells in both WT and *my15* (Figures 4E and 4E′). In both cases, a pseudopod is extended and separated from the cell body by laminar membranes. MOs successfully fuse with the PM in *my15*, consistent with immunostaining and MO fusion assay (Figures 4G′ and 4I′).

cil-1 may regulate membrane receptor localization in sperm. TRP-3/SPE-41 acts in sperm, translocates from MOs to the PM upon activation, and is required for fertilization [26]. In WT and *my15* spermatids, anti-TRP-3 labels cytoplasmic puncta partially overlapping with MOs (Figures 4H and 4I). In WT and *my15* spermatozoa, TRP-3 is detected ubiquitously on the PM of the pseudopod and cell body (Figures 5H″ and 5I″). *cil-1* is not required for TRP-3/TRPC translocation to the PM.

CIL-1 and PI 3-Kinase Activity Antagonistically Regulates Sperm Activation

Because PI biosensors show that CIL-1 hydrolyzes PI(3,4,5)P3 and PI(3,5)P2, we asked whether 3-kinase activity antagonizes CIL-1 5-phosphatase function. We applied 1 nM, 10 nM, and 100 nM wortmannin, a pharmacological inhibitor of PI 3-kinases that produce PI(3,4,5)P3 from PI(4,5)P2 [27], to WT and *my15* spermatids. At all concentrations tested, wortmannin acts as an in vitro activator of WT but not *my15* spermatids, with 100 nM being the most effective (compare Figure 4B‴ with Figure 4C‴). The low dose (1 nM) of wortmannin suggests specificity and indicates that PI 3-kinase activity and *cil-1* act antagonistically in sperm activation (Figures 5C and 5D).

Discussion

The PI 5-phosphatase CIL-1 mediates multiple aspects of *C. elegans* male reproductive biology (Figure 5). In male neurons, *cil-1* acts cell autonomously to control LOV-1 and PKD-2 localization but not function. Our data support a model whereby *cil-1* acts in early steps in TRPP complex downregulation by regulating PI(3)P distribution but not RAB-5 and STAM localization (Figures 5A and 5B). In sperm, *cil-1* positively regulates sperm activation and motility without affecting major membrane trafficking events. The 3-kinase inhibitor wortmannin is a potent sperm activator, which indicates that PI(3,4,5)P3 is a major CIL-1 substrate in sperm. We propose that one of the three 3-kinases encoded in the *C. elegans* genome (VPS-34, AGE-1, or F39B1.1) acts antagonistically to CIL-1 in a sperm activation pathway (Figures 5C and 5D).

cil-1 may be required for cellular polarity because distinct PI enrichment is a hallmark of polarized PM domains [28, 29]. However, *cil-1* mutants properly localize several other ciliary and presynaptic markers (Figure S1) and exhibit normal sensory behaviors, reflecting properly polarized and functional neurons. Alternatively, *cil-1* may modulate the activity of the TRPP complex. PI(4,5)P2 is a regulator of both TRP channel activity and trafficking [2]. Because *cil-1* mutant males exhibit normal mating behaviors, *cil-1* appears to regulate TRPP trafficking but not activity.

In neurons, *cil-1* regulates the balance between PI species that is important for intracellular polycystin trafficking. Although *cil-1* may negatively regulate polycystin insertion into the PM after initial targeting, our data are inconsistent with this model. A similar PKD-2::GFP Cil phenotype is observed in the adaptor protein 1 (AP-1) *unc-101(m1)* mutant background [14]. However, PKD-2::GFP particles are visibly moving along dendrites of both WT and *my15* (Movies S1 and S2) but not *unc-101* male sensory neurons (data not shown). Finally, PKD-2 abundance within ciliary regions is comparable between WT and *my15* (Figure 1, [16]).

Our data are most consistent with a requirement for CIL-1 in TRP-polycystin trafficking to early endosomes after endocytosis (Figure 5A and 5B). In RnB neurons, *cil-1* acts before STAM/Hrs-mediated receptor downregulation, which transport PKD-2 and LOV-1 from early endosomes to ESCRT [15]. In CEMs, it is difficult to place *lov-1*, *cil-1*, and *stam-1* in a pathway because of the additive phenotypes of double mutants. PI(3)P and PI(3,5)P2 balance in endocytic compartments is important for organelle maturation and receptor trafficking. In *cil-1(my15),* pre-early endosomal vesicles lacking the normal destination, the PI(3)P-enriched early endosomes, may simply accumulate and disperse along sensory neurons. Alternatively, *cil-1* may be required for maturation of endocytic compartments by affecting PI(3)P distribution, although this is unlikely given the normal localization of RAB-5 and STAM-1 in *my15* male sensory neurons. We propose that maintaining the balance between PI(3)P and PI(3,5)P2 by the CIL-1 5-phosphatase plays an essential role in polycystin trafficking between endocytic compartments.

Our data also reveal that *C. elegans* sperm activation is coordinated by the antagonistic actions of the CIL-1 5-phosphatase and an unidentified wortmannin-sensitive target. Although we cannot rule out off-target effects of wortmannin, we propose that CIL-1 and a PI3-kinase control PI(3,4,5)P3 levels. PI(3,4,5)P3 recruits and activates various effectors such as serine/threonine kinases and tyrosine kinases [30]. Cytoplasmic protein kinases and protein phosphatases are significantly overrepresented in *C. elegans* sperm [31]. Molecules such as SPE-6 serine/threonine kinase [32] may regulate sperm activation downstream of CIL-1-mediated turnover of PI(3,4,5)P3.

TRPP family members play important roles in mating and fertilization of numerous species [3, 7–12]. ADPKD male patients may exhibit infertility due to sperm immotility [33]. Sea urchin suREJ3 (receptor for egg jelly, a polycystin-1 homolog) and suPC2 (polycystin-2) localize to the PM proximal to acrosomal vesicles in sperm [8, 34]. In mice, PKD-REJ controls postcopulatory reproductive selection via effects

of TRP-3 (green) partially overlaps with 1CB4-labeled MOs. (H′) In WT spermatozoa, 1CB4-positive MOs are primarily located around the PM but absent from pseudopods (compare with bracket area in H″). (H″) In WT spermatozoa, anti-TRP-3 staining is detectable in the cell body and pseudopod PM (bracket). (H‴) An overlay of WT spermatozoa is shown. (I) In *my15* spermtids, MOs (red) are localized to the cell periphery just below the PM as in WT. Anti-TRP-3 staining (green) overlaps with MOs. (I′) In *my15* spermatozoa, similar to WT, MOs are found in the cell body but not pseudopod. (I″) In *my15* spermatozoa, TRP-3 protein is detected both in the cell body and in the pseudopod, as in WT. (I‴) An overlay of (H′) and (H″) with the DAPI image is shown.
The scale bars represents 5 μm.

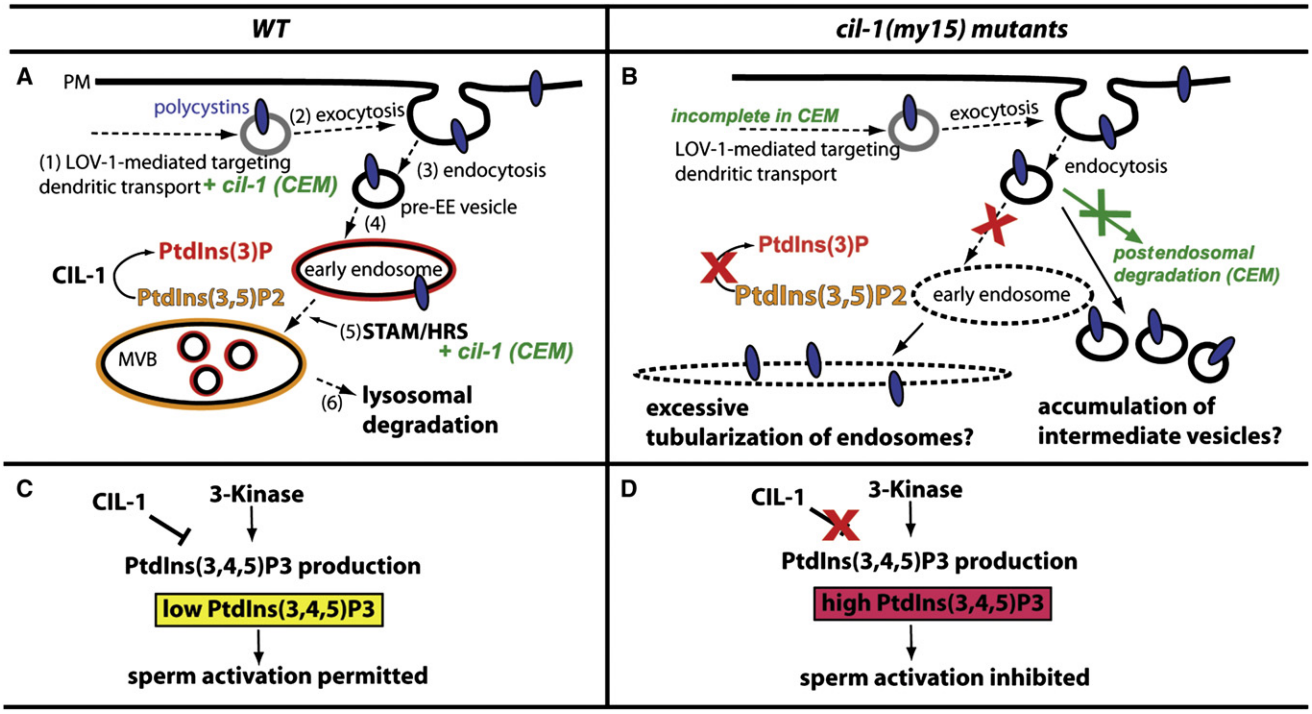

Figure 5. Models of CIL-1 Functions

(A and B) A model for CIL-1 function in polycystin trafficking in sensory neurons. (A) In WT RnB neurons, polycystins are (1) assembled in the cell body, transported along the dendrite, and (2) exocytosed at the PM, presumably at the ciliary base. Ciliary abundance of polycystins is tightly regulated by dynamic (3) internalization and endocytosis. (4) Pre-early endosomal (pre-EE) vesicles are sorted to PI(3)P-enriched (red lining) EE, followed by (5) targeting to multivesicular body (MVB). CIL-1 functions to maintain the balance between PI(3)P and PI(3,5)P2 in the EE and MVB membrane. Polycystin sorting from EE to MVB requires the STAM/Hrs complex. (6) Lysosomal degradation downregulates the polycystins. In CEM neurons, *cil-1* act at least partially in parallel with *lov-1* and *stam-1*, as indicated with green. (B) In *cil-1(my15)*, the Cil defect may occur after endocytosis. Loss of CIL-1 function causes depletion of PI(3)P, which in turn affects EE biogenesis and maturation. As shown in [38], pre-EE vesicles form an excessively tubularized EE along the microtubule network. Alternatively, polycystin-containing pre-EE vesicles may accumulate in neurons because their destination point [PI(3)P-enriched EE] is blocked. In *my15* CEM neurons, loss of *cil-1* affects dendritic targeting and postendosomal degradation (in green).

(C and D) A Model for CIL-1 function in sperm activation. (C) In a WT spermatozoon, lowering PI(3,4,5)P3 (yellow) by CIL-1 action initiates unidentified signaling pathway(s) to coordinate pseudopod extension and sperm movement. An unidentified 3-kinase that generates PI(3,4,5)P3 negatively regulates sperm activation. The balanced action between CIL-1 and 3-kinase maintains low levels of PI(3,4,5)P3, permitting sperm activation. (D) In *cil-1* mutant sperm, abnormally high PI(3,4,5)P3 levels inhibit downstream signaling pathways for pseudopod extension and sperm motility.

on sperm transport and exocytic competence during the acrosome reaction [11]. In the hermaphroditic chordate *Ciona intestinalis*, the *PKD1* homolog is expressed in testes and may act on sperm to control self-incompatibility [12]. In *Drosophila*, PKD2 may mediate sperm directional movement [9, 10]. Intriguingly, mutations in the type IV 5-phosphatase INPP5E gene cause human ciliary diseases [35, 36]. According to our phylogeny tree (Figure S2A), *cil-1* is the closest *C. elegans* homolog of INPP5E. Further experiments are needed to determine whether CIL-1 plays an evolutionarily conserved role in TRPP complex trafficking and sperm function in other species.

Supplemental Data

Supplemental Data include four figures, Supplemental Experimental Procedures, and four movies and can be found with this article online at http://www.cell.com/current-biology/supplemental/S0960-9822(09)01621-2.

Acknowledgments

Nancy L'Hernault provided assistance with electron microscopy. We thank Natalia Morsci, Jinghua Hu, and members of Barr laboratory for help throughout the course of this project; John Archibald, Ching Kung, and Andy Singson for helpful discussion; David Sherwood and Joshua Ziel for critical reading of the manuscript; Barth Grant for intestinal PI markers, Shawn X.-Y. Xu for the anti-TRP-3 antibody; and Sam Ward for sharing unpublished data. Some nematode strains used in this work were provided by the *Caenorhabditis* Genetics Center, which is funded by the National Institutes of Health (NIH) National Center for Research Resources (NCRR), and by Shohei Mitani of the National Bioresource Project for the Nematode (Japan). This work was supported by the NIH (DK059418 and DK074746 to M.M.B.; GM082932 to S.W.L.H.), the National Science Foundation (0131532 to S.W.L.H.), and the Polycystic Kidney Disease (PKD) Foundation (to M.M.B.).

Received: June 1, 2009
Revised: August 14, 2009
Accepted: August 17, 2009
Published online: September 24, 2009

References

1. Di Paolo, G., and De Camilli, P. (2006). Phosphoinositides in cell regulation and membrane dynamics. Nature *443*, 651–657.
2. Nilius, B., Owsianik, G., and Voets, T. (2008). Transient receptor potential channels meet phosphoinositides. EMBO J. *27*, 2809–2816.
3. Barr, M.M., and Sternberg, P.W. (1999). A polycystic kidney-disease gene homologue required for male mating behaviour in *C. elegans*. Nature *401*, 386–389.
4. Barr, M.M., DeModena, J., Braun, D., Nguyen, C.Q., Hall, D.H., and Sternberg, P.W. (2001). The *Caenorhabditis elegans* autosomal

dominant polycystic kidney disease gene homologs *lov-1* and *pkd-2* act in the same pathway. Curr. Biol. *11*, 1341–1346.

5. Igarashi, P., and Somlo, S. (2002). Genetics and pathogenesis of polycystic kidney disease. J. Am. Soc. Nephrol. *13*, 2384–2398.
6. Bae, Y.K., and Barr, M.M. (2008). Sensory roles of neuronal cilia: Cilia development, morphogenesis, and function in *C. elegans*. Front. Biosci. *13*, 5959–5974.
7. Huang, K., Diener, D.R., Mitchell, A., Pazour, G.J., Witman, G.B., and Rosenbaum, J.L. (2007). Function and dynamics of PKD2 in *Chlamydomonas* flagella. J. Cell Biol. *179*, 501–514.
8. Neill, A.T., Moy, G.W., and Vacquier, V.D. (2004). Polycystin-2 associates with the polycystin-1 homolog, suREJ3, and localizes to the acrosomal region of sea urchin spermatozoa. Mol. Reprod. Dev. *67*, 472–477.
9. Gao, Z., Ruden, D.M., and Lu, X. (2003). PKD2 cation channel is required for directional sperm movement and male fertility. Curr. Biol. *13*, 2175–2178.
10. Watnick, T.J., Jin, Y., Matunis, E., Kernan, M.J., and Montell, C. (2003). A flagellar polycystin-2 homolog required for male fertility in *Drosophila*. Curr. Biol. *13*, 2179–2184.
11. Sutton, K.A., Jungnickel, M.K., and Florman, H.M. (2008). A polycystin-1 controls postcopulatory reproductive selection in mice. Proc. Natl. Acad. Sci. USA *105*, 8661–8666.
12. Harada, Y., Takagaki, Y., Sunagawa, M., Saito, T., Yamada, L., Taniguchi, H., Shoguchi, E., and Sawada, H. (2008). Mechanism of self-sterility in a hermaphroditic chordate. Science *320*, 548–550.
13. L'Hernault, S.W. (2006). Spermatogenesis. In WormBook, The *C. elegans* Research Community, ed. 10.1895/wormbook.1.7.1, http://www.wormbook.org.
14. Bae, Y.K., Qin, H., Knobel, K.M., Hu, J., Rosenbaum, J.L., and Barr, M.M. (2006). General and cell-type specific mechanisms target TRPP2/PKD-2 to cilia. Development *133*, 3859–3870.
15. Hu, J., Wittekind, S.G., and Barr, M.M. (2007). STAM and Hrs down-regulate ciliary TRP receptors. Mol. Biol. Cell *18*, 3277–3289.
16. Bae, Y.K., Lyman-Gingerich, J., Barr, M.M., and Knobel, K.M. (2008). Identification of genes involved in the ciliary trafficking of *C. elegans* PKD-2. Dev. Dyn. *237*, 2021–2029.
17. Nonet, M.L. (1999). Visualization of synaptic specializations in live *C. elegans* with synaptic vesicle protein-GFP fusions. J. Neurosci. Methods *89*, 33–40.
18. Gurung, R., Tan, A., Ooms, L.M., McGrath, M.J., Huysmans, R.D., Munday, A.D., Prescott, M., Whisstock, J.C., and Mitchell, C.A. (2003). Identification of a novel domain in two mammalian inositol-polyphosphate 5-phosphatases that mediates membrane ruffle localization. The inositol 5-phosphatase skip localizes to the endoplasmic reticulum and translocates to membrane ruffles following epidermal growth factor stimulation. J. Biol. Chem. *278*, 11376–11385.
19. Bui, Y.K., and Sternberg, P.W. (2002). *Caenorhabditis elegans* inositol 5-phosphatase homolog negatively regulates inositol 1,4,5-triphosphate signaling in ovulation. Mol. Biol. Cell *13*, 1641–1651.
20. Gower, N.J., Walker, D.S., and Baylis, H.A. (2005). Inositol 1,4,5-trisphosphate signaling regulates mating behavior in *Caenorhabditis elegans* males. Mol. Biol. Cell *16*, 3978–3986.
21. Harris, T.W., Hartwieg, E., Horvitz, H.R., and Jorgensen, E.M. (2000). Mutations in synaptojanin disrupt synaptic vesicle recycling. J. Cell Biol. *150*, 589–600.
22. Roggo, L., Bernard, V., Kovacs, A.L., Rose, A.M., Savoy, F., Zetka, M., Wymann, M.P., and Muller, F. (2002). Membrane transport in *Caenorhabditis elegans*: an essential role for VPS34 at the nuclear membrane. EMBO J. *21*, 1673–1683.
23. Christoforidis, S., Miaczynska, M., Ashman, K., Wilm, M., Zhao, L., Yip, S.C., Waterfield, M.D., Backer, J.M., and Zerial, M. (1999). Phosphatidylinositol-3-OH kinases are Rab5 effectors. Nat. Cell Biol. *1*, 249–252.
24. Okamoto, H., and Thomson, J.N. (1985). Monoclonal antibodies which distinguish certain classes of neuronal and supporting cells in the nervous tissue of the nematode *Caenorhabditis elegans*. J. Neurosci. *5*, 643–653.
25. Washington, N.L., and Ward, S. (2006). FER-1 regulates Ca2+ -mediated membrane fusion during *C. elegans* spermatogenesis. J. Cell Sci. *119*, 2552–2562.
26. Xu, X.-Z.S., and Sternberg, P.W. (2003). A *C. elegans* sperm TRP protein required for sperm-egg interactions during fertilization. Cell *114*, 285–297.
27. Arcaro, A., and Wymann, M.P. (1993). Wortmannin is a potent phosphatidylinositol 3-kinase inhibitor: the role of phosphatidylinositol 3,4,5-trisphosphate in neutrophil responses. Biochem. J. *296*, 297–301.
28. Shi, S.-H., Jan, L.Y., and Jan, Y.-N. (2003). Hippocampal neuronal polarity specified by spatially localized mPar3/mPar6 and PI 3-kinase activity. Cell *112*, 63–75.
29. Pinal, N., Goberdhan, D.C., Collinson, L., Fujita, Y., Cox, I.M., Wilson, C., and Pichaud, F. (2006). Regulated and polarized PtdIns(3,4,5)P3 accumulation is essential for apical membrane morphogenesis in photoreceptor epithelial cells. Curr. Biol. *16*, 140–149.
30. Hawkins, P.T., Anderson, K.E., Davidson, K., and Stephens, L.R. (2006). Signalling through Class I PI3Ks in mammalian cells. Biochem. Soc. Trans. *34*, 647–662.
31. Reinke, V., Smith, H.E., Nance, J., Wang, J., Van Doren, C., Begley, R., Jones, S.J., Davis, E.B., Scherer, S., Ward, S., and Kim, S.K. (2000). A global profile of germline gene expression in *C. elegans*. Mol. Cell *6*, 605–616.
32. Muhlrad, P.J., and Ward, S. (2002). Spermiogenesis initiation in *Caenorhabditis elegans* involves a casein kinase 1 encoded by the *spe-6* gene. Genetics *161*, 143–155.
33. Vora, N., Perrone, R., and Bianchi, D.W. (2008). Reproductive issues for adults with autosomal dominant polycystic kidney disease. Am. J. Kidney Dis. *51*, 307–318.
34. Mengerink, K.J., Moy, G.W., and Vacquier, V.D. (2002). suREJ3, a polycystin-1 protein, is cleaved at the GPS domain and localizes to the acrosomal region of sea urchin sperm. J. Biol. Chem. *277*, 943–948.
35. Bielas, S.L., Silhavy, J.L., Brancati, F., Kisseleva, M.V., Al-Gazali, L., Sztriha, L., Bayoumi, R.A., Zaki, M.S., Abdel-Aleem, A., Rosti, R.O., et al. (2009). Mutations in INPP5E, encoding inositol polyphosphate-5-phosphatase E, link phosphatidyl inositol signaling to the ciliopathies. Nat Genet. *41*, 1032–1036.
36. Jacoby, M., Cox, J.J., Gayral, S., Hampshire, D.J., Ayub, M., Blockmans, M., Pernot, E., Kisseleva, M.V., Compere, P., Schiffmann, S.N., et al. (2009). INPP5E mutations cause primary cilium signaling defects, ciliary instability and ciliopathies in human and mouse. Nat Genet. *41*, 1027–1031.
37. Hu, J., Bae, Y.K., Knobel, K.M., and Barr, M.M. (2006). Casein kinase II and calcineurin modulate TRPP function and ciliary localization. Mol. Biol. Cell *172*, 2200–2211.
38. Fili, N., Calleja, V., Woscholski, R., Parker, P.J., and Larijani, B. (2006). Compartmental signal modulation: Endosomal phosphatidylinositol 3-phosphate controls endosome morphology and selective cargo sorting. Proc. Natl. Acad. Sci. USA *103*, 15473–15478.